Journal of Solid State Chemistry **160,** 293–301 (2001)
doi:10.1006/jssc.2001.9198, available online at http://www.idealibrary.com on IDEAL®

Synthesis, Crystal Structure, and Magnetic Properties of Quasi-One-Dimensional Oxides Ca_3CuMnO_6 and $Ca_3Co_{1+x}Mn_{1-x}O_6$

V. G. Zubkov, G. V. Bazuev,[1] A. P. Tyutyunnik, and I. F. Berger

Institute of Solid State Chemistry, Ural Branch of the Russian Academy of Sciences, Ekaterinburg, 620219, Russia

Received November 15, 2000; in revised form March 22, 2001; accepted April 9, 2001; published online July 16, 2001

Synthesis conditions, crystal structures, and magnetic properties of quasi-one-dimensional complex oxides Ca_3CuMnO_6 (space group *P*-1, $z = 4$, triclinic cell) and $Ca_3Co_{1+x}Mn_{1-x}O_6$ with $x = 0$, 0.25, 1.0 (structural type K_4CdCl_6, space group *R*-3*c*, $z = 6$) are presented. The crystal structures of Ca_3CoMnO_6 and Ca_3CuMnO_6 were refined using neutron and combined X-ray and neutron diffraction analysis, respectively. The interatomic distances in oxygen polyhedra were found. In contrast to ferromagnetic $Ca_3Co_2O_6$ ($T_C = 24$ K), manganese-containing phases $Ca_3Co_{1+x}Mn_{1-x}O_6$ are characterized by antiferromagnetic interactions with Neel temperatures 18 K ($x = 0.25$) and 13 K ($x = 0$). For Ca_3CuMnO_6 T_N was established to be 6 K. © 2001 Academic Press

Key Words: **low-dimensional oxides; X-ray diffraction; neutron scattering; magnetic properties.**

INTRODUCTION

A new series of complex oxides Ca_3AMnO_6 (A = Cu, Ni, Zn) with K_4CdCl_6-type structure has been obtained (1–4). A distinguishing feature of Ca_3NiMnO_6 and Ca_3ZnMnO_6 structures is the presence of infinite chains consisting of face-shared MnO_6 octahedra and AO_6 trigonal prisms (A = Ni, Zn). These structural units lie along the hexagonal *c*-axis and are surrounded by six chains made of Ca antiprisms. Such a structure of the oxides under consideration allows us to characterize them from the structural viewpoint as quasi-one-dimensional ones. The crystal structure of these oxides is related to that of Sr_3APtO_6 and Sr_3AIrO_6 (5, 6). An analogous structure was found for the complex oxide $Ca_3Co_2O_6$ (7) in which both octahedral and prismatic sites are occupied by Co cations.

The quasi-one-dimensional character of the structure of the analyzed compounds determines the pronounced anisotropy of their physical and especially magnetic properties. Depending on the electronic configuration of transition metal cations constituting one-dimensional chains, substances with different magnetic properties were found among these compounds—antiferromagnetics, ferromagnetics, and ferrimagnetics. The temperature of magnetic ordering in them is rather low. The magnetic susceptibility of the considered oxides is described either by the 1D paramagnetic Heisenberg model or by the 1D Ising model. In the case of the solid solution $Sr_3CuPt_{0.5}Ir_{0.5}O_6$, the magnetic behavior was explained by the disordered spin–chain paramagnetism model (5). The compound $Ca_3Co_2O_6$ undergoes ferrimagnetic ordering below 24 K (8) as a result of ferromagnetic exchange interactions between Co cations inside the chains and antiferromagnetic interactions between the chains. Manganese analogues of these oxides—Ca_3AMnO_6 where $A = Zn^{2+}$, Ni^{2+}—are characterized by antiferromagnetic interactions at low temperatures (1–4).

In this paper we report the synthesis, crystal structure, and magnetic properties of Ca_3CuMnO_6, Ca_3CoMnO_6, and $Ca_3Co_{1.25}Mn_{0.75}O_6$ oxides. The two latter compounds are analyzed in comparison with $Ca_3Co_2O_6$.

EXPERIMENTAL

Ca_3CuMnO_6 and $Ca_3Co_{1+x}Mn_{1-x}O_6$ samples were synthesized via solid state reactions from high-purity calcium carbonate $CaCO_3$ and MnO_2, CuO, and CoO oxides containing a minimum of 99.9% of the main substance. The mixtures of initial substances were pressed into pellets and annealed first at 950°C for 30 h and then at 1000°C ($Ca_3Co_2O_6$), 1130°C (Ca_3CuMnO_6), or 1200°C (Ca_3CoMnO_6 and $Ca_3Co_{1.25}Mn_{0.75}O_6$) for 24 h. A lower temperature of $Ca_3Co_2O_6$ synthesis is required because it decomposes at 1036°C (7). The final treatment of the samples was performed in an oxygen atmosphere at 1000°C for 4 h with subsequent slow cooling. The phase composition of the sintering products was controlled by X-ray powder diffraction analysis with a DRON-2 diffractometer using Cu$K\alpha$ radiation.

X-ray diffraction data were obtained at room temperature in Cu$K\alpha$ radiation using the automatic diffractometer

[1] To whom correspondence should be addressed. E-mail: bazuev@ihim.uran.ru.

0022-4596/01 $35.00

STADI-P (STOE, Germany). X-ray diffraction patterns were taken by points in the angle interval 2θ from 5° to 120° with a step of 0.02°. Neutron diffraction data were collected from 5–105° 2θ with a step of 0.1° and neutron wavelength $\lambda = 1.8031$ Å using a D2A setup of the reactor IVV 2M (Zarechny). These data were employed in the calculations.

The crystal structure of Ca_3CuMnO_6 was refined on the basis of combined X-ray and neutron diffraction data using a program of full-profile analysis according to Rietveld's GSAS program (9).

The oxygen content in the samples was determined by thermogravimetric analysis (TGA) in hydrogen flow at 900°C. In the calculations it was taken into account that Cu and Co in the reduction products appeared as metals, while Mn was reduced to the bivalent state. In accordance with TGA data, the oxygen content in monophase samples was close to stoichiometry and corresponded to an index 6.00 ± 0.03.

Magnetic measurements were obtained using an MPMS SQUID magnetometer at temperatures from 2 to 300 K. Magnetic susceptibility was measured in magnetic fields of 0.5, 5, and 8.9 kOe after the samples were cooled in zero and measured magnetic fields. Magnetization measurements were performed in magnetic fields from 1 to 50 kOe at temperatures below and above the magnetic ordering point.

RESULTS AND DISCUSSION

Initial mixtures of Mn, Co oxides and $CaCO_3$ taken in ratios corresponding to the formula $Ca_3Co_{1+x}Mn_{1-x}O_6$ ($x = 0$, 0.25, 0.5, 1.0, -0.25) were annealed to prepare monophase samples with $x = 0$, 0.25, 1.0 as determined by X-ray diffraction studies. Impurity phases in the remaining samples were detected irrespective of the synthesis temperature. The presence of both $Ca_3Co_2O_6$ and $Ca_3Co_{1.25}Mn_{0.75}O_6$ in the samples with $x = 0.5$ indicates that there is no complete mutual solubility between the final phases of the analyzed system ($Ca_3Co_2O_6$ and Ca_3CoMnO_6). This can be associated with essential differences in the preferences of cobalt and manganese cations to occupy available crystallographic positions, as well as with individual features of these compounds.

Figure 1 displays X-ray diffraction patterns of Ca_3CoMnO_6 which were indexed, like in the case of $Ca_3Co_{1.25}Mn_{0.75}O_3$, in a hexagonal symmetry in the $R-3c$ space group (K_4CdCl_6-type structure). Table 1 lists the unit cell parameters of the obtained compounds in the rhombohedral symmetry, parameters of isostructural oxides Ca_3AMnO_6, where A = Ni, Zn (1–4), and ionic radii of A^{2+} cations (10).

As follows from Table 1, the lattice parameters of both Mn-containing phases considerably exceed those for $Ca_3Co_2O_6$ which is likely to result from larger dimensions of Mn cations as compared with Co cations. This conclusion is confirmed by intermediate values of $Ca_3Co_{1.25}Mn_{0.75}O_6$ parameters. Comparison of the parameters for Ca_3CoMnO_6 and Ca_3AMnO_6 where A = Ni, Zn shows that their dependence on the ionic radius of the d-element bivalent cation agrees with the increase in the dimension of the latter radii only in the series Ni^{2+}–Zn^{2+}. The Co-containing phase is characterized by lattice parameters only slightly exceeding the parameters of Ca_3NiMnO_6 although cobalt has the largest ionic radius among the considered bivalent cations. Perhaps this is associated with the earlier established (4) partial (8%) replacement of Ni^{2+} by Mn^{2+} cations with a larger ionic radius [0.83 Å (10)] which takes place in trigonal prisms.

The structure of Sr_3NiIrO_6 (6) was used as an initial model for neutron diffraction refinement of the structure of Ca_3CoMnO_6. In this model (space group $R-3c$, $z = 6$) large-size ions (cobalt ions) are localized in the centers of trigonal prisms (6a positions) and smaller ions (manganese ions) in octahedra (6b positions). Alkaline earth elements are

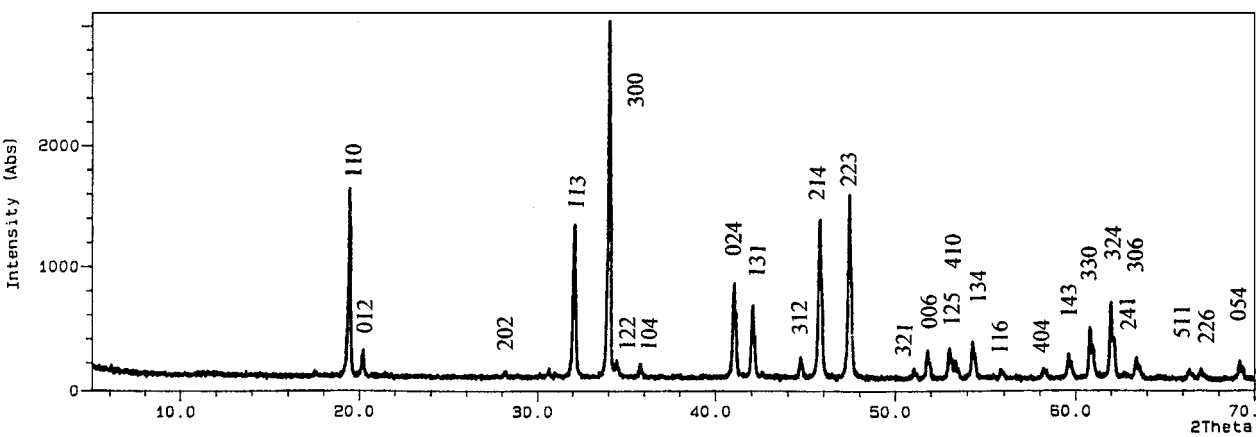

FIG. 1. X-ray diffraction patterns of Ca_3CoMnO_6.

TABLE 1
Unit Cell Parameters of $Ca_3Co_{1+x}Mn_{1-x}O_6$ and Ca_3AMnO_6 (A = Co, Zn, Ni)

Compound	a, Å	c, Å	V, Å^3	$R(A^{2+})$, Å
$Ca_3Co_2O_6$	9.0776(1)	10.3817(1)	740.87	
$Ca_3Co_{1.25}Mn_{0.75}O_6$	9.1257(11)	10.5517(20)	761.01(19)	
Ca_3CoMnO_6	9.1314(1)	10.5817(1)	764.12(5)	0.745
Ca_3ZnMnO_6	9.1443(6)	10.6318(13)	769.91(12)	0.74
Ca_3NiMnO_6	9.1227(10)	10.5811(17)	762.62(18)	0.69

TABLE 2
Structural Parameters for Ca_3CoMnO_6 at 293 K (Standard Deviation in Parentheses)

Atom	Site	X/a	Y/b	Z/c	B_{iso} Å^2
Ca	18*e*	0.3621(1)	0.0	$\frac{1}{4}$	0.70(6)
Mn	6*b*	0.0	0.0	0.0	0.26(5)
Co	6*a*	0.0	0.0	$\frac{1}{4}$	0.98(5)
O	36*f*	0.1779(2)	0.0247(2)	0.1080(1)	0.64(4)

Note. $R_1 = 5.1\%$, $R_{pf} = 5.37\%$, $R_{wp} = 5.07\%$.

positioned in square antiprisms with coordination number 8 (18 e) and oxygen atoms occupy 36*f* sites.

The refinement performed shows that 6*b* sites in the Ca_3CoMnO_6 structure are occupied by Mn. Co atoms are localized in 6*a*, calcium in 18*e*, and oxygen in 36*f* sites. The results of the refinement are given in Table 2. The experimental and difference neutron diffraction patterns, as well as a calculated stroke diagram, are presented in Fig. 2. On the basis of these data and the crystal lattice parameters of Ca_3CoMnO_6 (Table 1) we have calculated interatomic distances in oxygen polyhedra. The Co–O bonding length (2.140 Å) is close to that found for Ni–O in Ca_3NiMnO_6 [2.137 Å (3)]. The Mn–O distance (1.905 Å) is in a very good agreement with those observed in the perovskite β-$SrMnO_3$ [1.903 Å (11)], β-Sr_2MnO_4 [1.894 Å (12)], and Ca_3NiMnO_6 [1.905 Å (3)]. The Ca–O bonding lengths in the square antiprism CaO_8 equal $2.349(1)\times 2$, $2.463(1)\times 2$, $2.468(2)\times 2$, and $2.619(1)\times 2$. Allowing for the empirical relationships "bonding length – bonding tension" (13) we estimated the degrees of cation oxidation to be 3.9(1) for Mn, 1.8(2) for Co, and 1.9(2) for Ca. The results obtained support the conclusion that the compound under analysis contains in its structural motif isolated chains of the form–Mn^{4+}–Co^{2+}–Mn^{4+}–Co^{2+}– etc.

Interatomic distances Co–Mn inside the chains amount to 2.645 Å. This small value results from the fact that octahedra with Mn cations and Co-containing trigonal prisms which alternate in finite chains share faces with each other. The presence of rather short Mn–Co distances, however, does not lead to the formation of metal–metal bonds and according to specific electroresistance measurements this substance is an insulator.

The results of magnetic susceptibility measurements for the obtained three complex oxides given in Fig. 3 bear witness to the ferromagnetic nature of the compound $Ca_3Co_2O_6$ with $T_K = 24$ K. The replacement of 37.5 and 50% of Co by Mn brings about a transition from ferromagnetic to antiferromagnetic exchange interaction between paramagnetic atoms in the chains. This is also confirmed by the change in the sign of the Weiss's constant θ from

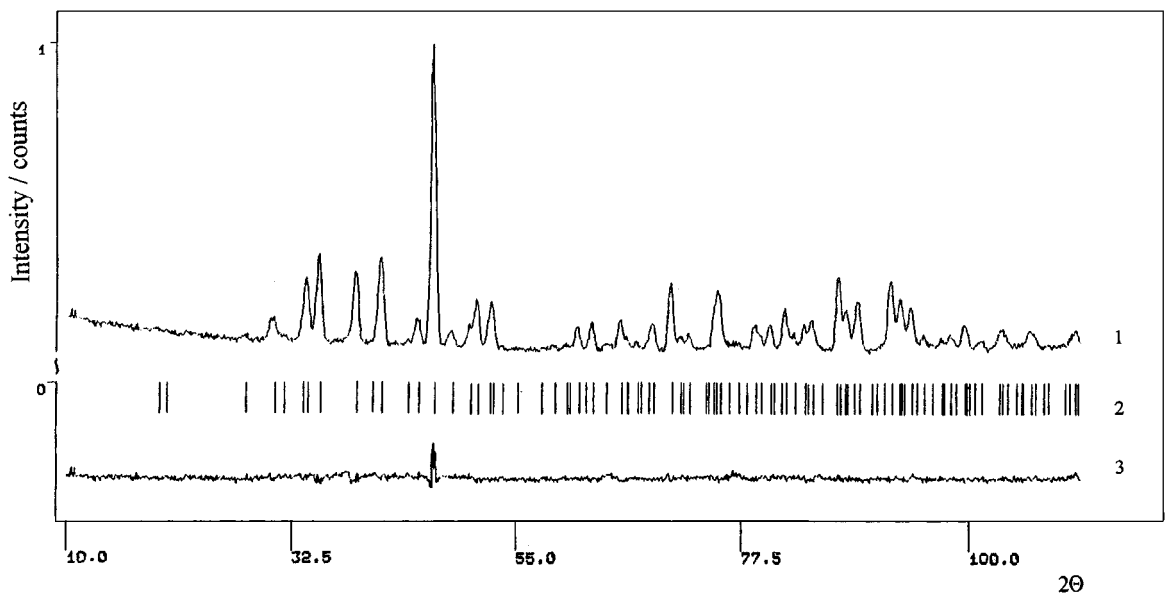

FIG. 2. Neutron Rietveld analysis for Ca_3CoMnO_6 at 293 K showing (1) the observed, (2) calculated, and (3) difference patterns.

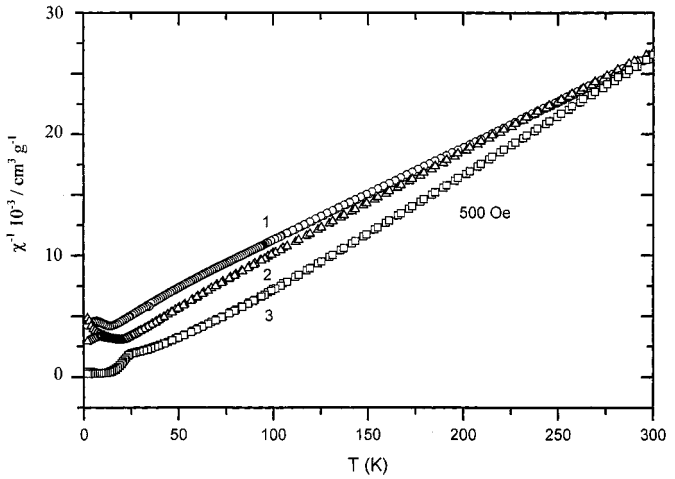

FIG. 3. Inverse magnetic susceptibility χ as a function of temperature for (1) Ca_3CoMnO_6, (2) $Ca_3Co_{1.25}Mn_{0.75}O_6$, and (3) $Ca_3Co_2O_6$.

a positive value for $Ca_3Co_2O_6$ (+ 30 K) to negative ones of $Ca_3Co_{1.25}Mn_{0.75}O_6$ (− 20 K) and Ca_3CoMnO_6 (− 45 K), as well as by the absence of spontaneous magnetic moment in the latter compound at temperatures below the magnetic transformation point. Neel temperatures found by maxima on $\chi = f(T)$ curves are equal to 18 and 13 K for $Ca_2Co_{1.25}Mn_{0.75}O_6$ and Ca_3CoMnO_6, respectively. To elucidate the possibility of establishing a long-range magnetic order at low temperatures, we performed neutron diffraction studies of Ca_3CoMnO_6 at 4.2 K. The findings, however, pointed only to the presence of a short-range order in the arrangement of magnetic moments of cations: instead of clear-cut magnetic reflections, the diffraction pattern contained additional wide low-intensity peaks.

The magnetic susceptibility of all examined compounds obeys the Curie–Weiss law $\chi = C/(T - \theta)$ at temperatures above 75–120 K (Fig. 3). Experimental values of constants C, θ, and magnetic moments μ_{exp} are listed in Table 3. According to (8), cobalt atoms in $Ca_3Co_2O_6$ occupying octahedral sites are in the low-spin trivalent state Co^{3+} (LS), while those positioned in trigonal prismatic sites are in the high-spin trivalent state Co^{3+} (HS). The resultant magnetic moment calculated in conformity with the electronic configurations of these cations is 4.90 μ_B per formula unit which closely agrees with the experimental value μ_{exp} (5.17 μ_B) for our sample $Ca_3Co_2O_6$. For Ca_3CoMnO_6, the experimental values of μ_{exp} and C are in satisfactory agreement with the values calculated for two types of cation combinations Co^{2+}(HS)–Mn^{4+} and Co^{3+}(HS)–Mn^{3+}(LS). For the first combination, large experimental values of μ_B and C as compared with the calculated estimates (see Table 3) can be explained by incomplete freezing of the orbital component of the magnetic moment for Co^{2+} (14). The second combination agrees with the experimental data provided that high-spin cations Co^{3+} occupy trigonal prismatic sites like in $Ca_3Co_2O_6$, whereas Mn^{3+}(LS) cations having smaller dimensions are localized in octahedral sites. Considering the results of structural investigations, it may be inferred that the cation combination Co^{2+}(HS)–Mn^{4+} is present in this oxide. This explains the fact established in the process of synthesis that there is no complete mutual solubility between $Ca_3Co_2O_6$ and Ca_3CoMnO_6. Unlimited solubility suggests the presence of different-valence cations in both prismatic and octahedral sites: the former sites should be occupied by Co^{3+}(HS) along with Co^{2+} cations, while the latter ones should be occupied by Mn^{4+} and Co^{3+}(LS) cations. Such a situation seems to be unlikely in view of the dimension factor.

Our conclusion about the cation combination is in conformity with the data reported in (15, 16) where the magnetic properties of $LnCo_{0.5}Mn_{0.5}O_3$ perovskites (Ln = rare-earth element) are explained in terms of an indirect exchange interaction between Co^{2+} and Mn^{4+} cations. Taking into account the foregoing concepts and the results of comparative analysis between the experimental and calculated values of Curie's constants and magnetic moments, it may be suggested that cobalt and manganese in $Ca_3Co_{1.25}Mn_{0.75}O_6$ are also mainly in the bi- and tetravalent states, respectively. Some cobalt ions are possibly in the form of low-spin cations Co^{3+}(LS) in the octahedra. In this case Co^{3+}(HS) cations are partially present in the prisms alongside Co^{2+}. This assumption is indirectly supported by research on the magnetic properties of $Ca_3Co_{1.25}Mn_{0.75}O_6$. Magnetization measurements, for example, show that for $Ca_3Co_{1.25}Mn_{0.75}O_6$ below the magnetic transition point there is a noticeable discrepancy between the values obtained when the samples were cooled in measured and zero magnetic fields (Fig. 4). As for Ca_3CoMnO_6, this discrepancy is very insignificant. In addition to that, at 2 and 15 K the magnetization versus applied magnetic field dependence for $Ca_3Co_{1.25}Mn_{0.75}O_6$ was detected to deviate from a straight line (Fig. 5) which may imply the existence of a ferromagnetic component at temperatures below the magnetic ordering point. However, it should be pointed out that some nonlinearity is also

TABLE 3
Magnetic Properties of $Ca_3Co_{1+x}Mn_{1-x}O_6$

Compound	C, mol^{-1}	Θ, K	C_{calc}, mol^{-1}	μ_{exp}, μ_B	μ_{calc}
$Ca_3Co_2O_6$	3.34	+ 30	3.0	5.17	4.90
$Ca_3Co_{1.25}Mn_{0.75}O_6$	3.85	− 20	3.37 (Co^{2+}HS–Co^{3+}LS–Mn^{4+})	5.55	5.20
Ca_3CoMnO_6	4.24	− 45	3.75 (Co^{2+}HS–Mn^{4+})	5.82	5.48
			4.0 (Co^{3+}HS–Mn^{3+}LS)		5.67

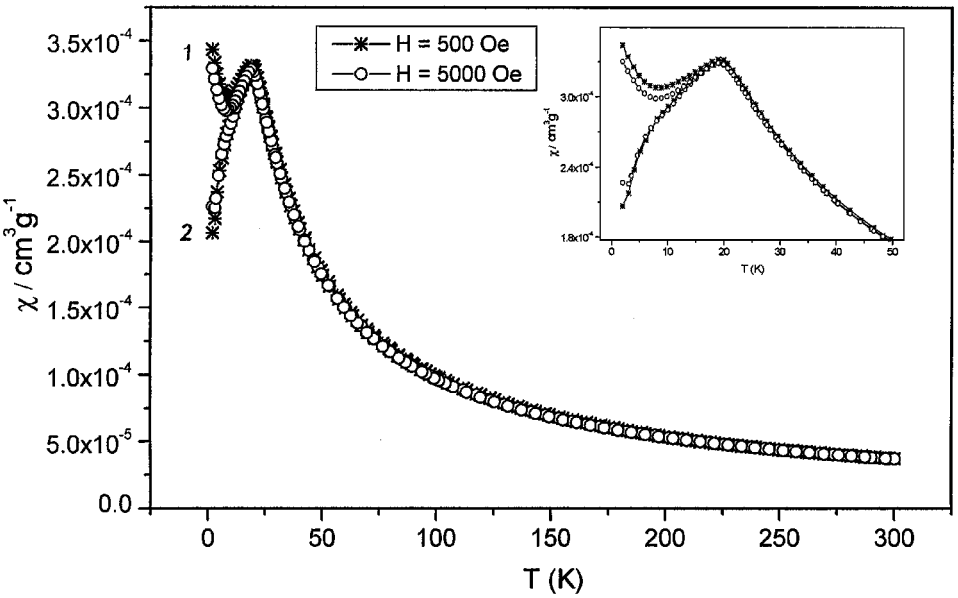

FIG. 4. Magnetic susceptibility χ as a function of temperature for $Ca_3Co_{1.25}Mn_{0.75}O_6$ after cooling the sample (1) in measured and (2) zero magnetic field.

observed for the analogous dependence for Ca_3CoMnO_6 (Fig. 6).

Originally the structure of Sr_3NiIrO_6 (4, 5) was used as an initial model for refining the crystal structure of Ca_3CuMnO_6, as was the case with Ca_3CoMnO_6. Structural refinement with the use of these data yielded no results since the difference X-ray diffraction pattern contained diffraction lines forbidden in the R–3c space group. Refinement parameters were essentially improved when the structure of Sr_3CuPtO_6 (17, 18) with a monoclinic lattice (space group $C2/c$, $z = 4$) was used as a model. In this compound strontium occupies 4e and 8f, copper 4e, platinum 4c, and three types of oxygen atoms 8f sites. The coordination of copper atoms in Sr_3CuPtO_6 changes from trigonal prismatic to

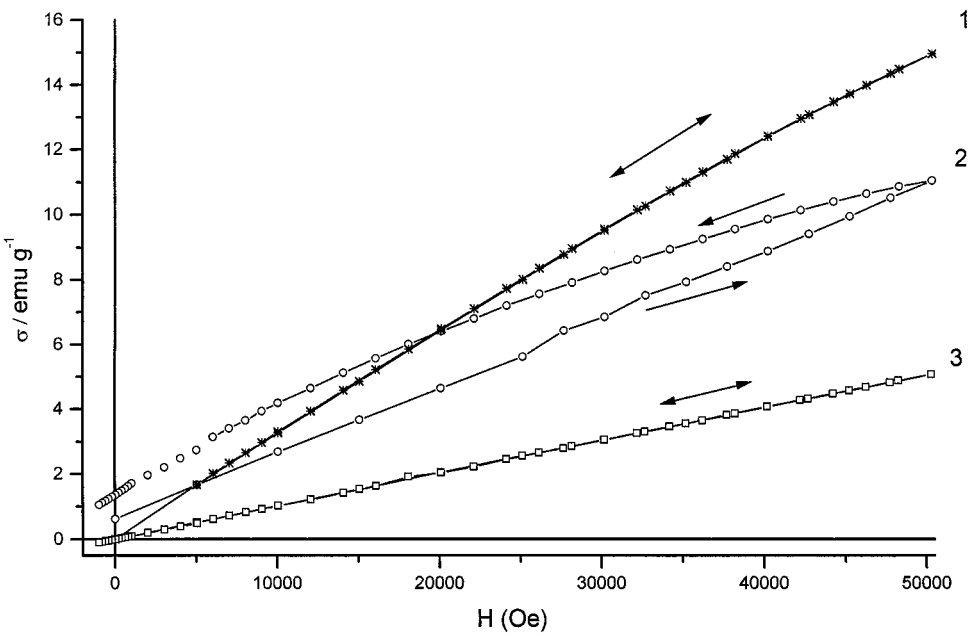

FIG. 5. Magnetization σ of $Ca_3Co_{1.25}Mn_{0.75}O_6$ as a function of applied magnetic field at (1) 15, (2) 2, and (3) 100 K.

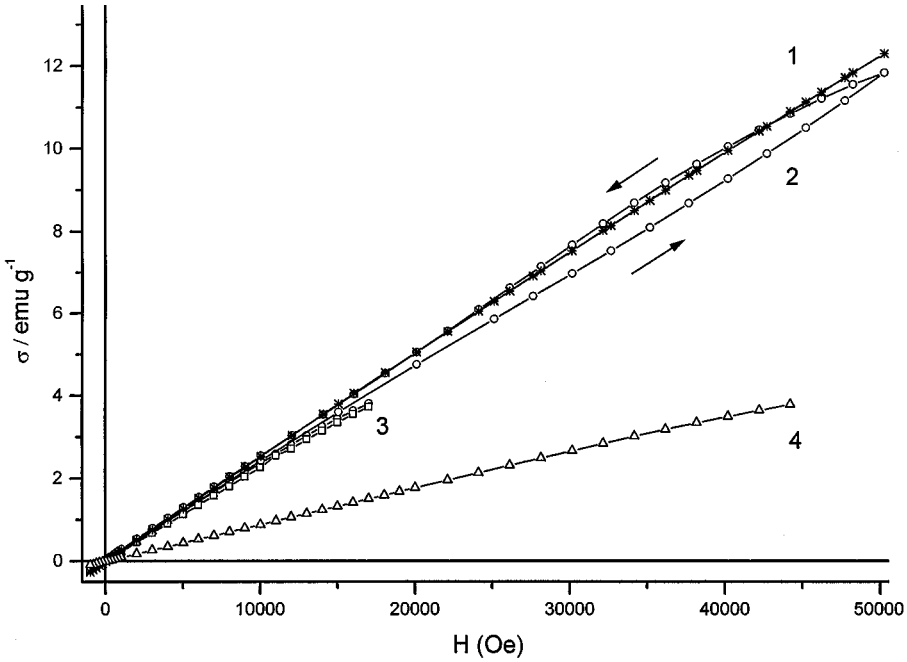

FIG. 6. Magnetization σ of Ca_3CoMnO_6 as a function of applied magnetic field at (1) 15, (2) 2, (3) 10, and (4) 100 K.

square planar because they were displaced from the center of the prisms to one of the rectangular faces of the coordination polyhedron. Mn atoms in this model remain in octahedral sites. However, the model failed too. Although the minimum was reached, the computational and experimental diffraction patterns differed substantially. The latter contained additional lines incompatible with either $C2/c$ and $P2/c$ (subgroup of the $C2/c$ group) or $P2/m$ space groups.

TABLE 4
Structural Parameters for Ca_3CuMnO_6 at 295 K

Atom	Site	x	y	z	U_{iso}	Fract.
Ca1	2*i*	0.3097(19)	0.0748(18)	0.6144(23)	1.34(6)	1.0
Ca2	2*i*	− 0.3202(21)	0.0711(18)	− 0.1053(25)	1.34(6)	1.0
Ca3	2*i*	0.8152(20)	0.5695(19)	0.6093(24)	1.34(6)	1.0
Ca4	2*i*	0.1772(19)	0.5609(18)	− 0.1221(23)	1.34(6)	1.0
Ca5	2*i*	− 0.0040(19)	0.1122(17)	0.2555(26)	1.34(6)	1.0
Ca6	2*i*	0.5019(20)	0.6109(15)	0.2544(24)	1.34(6)	1.0
Mn1	2*i*	0.2532(14)	0.2477(18)	− 0.0075(18)	1.59(7)	1.0
Mn2	2*i*	0.7483(14)	0.2428(18)	0.4987(18)	1.59(7)	1.0
Cu1	2*i*	0.4877(11)	0.2634(10)	0.2785(14)	1.59(7)	0.902 (11)
Mn3	2*i*	0.4877(11)	0.2634(10)	0.2785(14)	1.59(7)	0.098 (11)
Cu2	2*i*	0.0299(10)	0.7760(11)	0.1812(14)	1.59(7)	1.000 (15)
O1	2*i*	0.2235(21)	0.3326(23)	0.7121(34)	0.46(6)	1.0
O2	2*i*	− 0.2175(24)	0.3263(19)	− 0.2275(32)	0.46(6)	1.0
O3	2*i*	0.7410(22)	0.8006(21)	0.7198(26)	0.46(6)	1.0
O4	2*i*	0.2562(23)	0.8027(23)	− 0.2128(29)	0.46(6)	1.0
O5	2*i*	0.3692(27)	0.4264(23)	0.0759(37)	0.46(6)	1.0
O6	2*i*	− 0.8557(24)	0.4206(21)	0.4051(32)	0.46(6)	1.0
O7	2*i*	0.8557(24)	0.9236(23)	0.0707(35)	0.46(6)	1.0
O8	2*i*	0.1421(25)	0.9058(18)	0.4136(30)	0.46(6)	1.0
O9	2*i*	0.06149(23)	0.3517(21)	0.0355(33)	0.46(6)	1.0
O10	2*i*	− 0.637(24)	0.3472(22)	0.4625(32)	0.46(6)	1.0
O11	2*i*	0.5620(26)	0.8565(19)	0.0392(30)	0.46(6)	1.0
O12	2*i*	0.4450(25)	0.8607(21)	0.4558(33)	0.46(6)	1.0

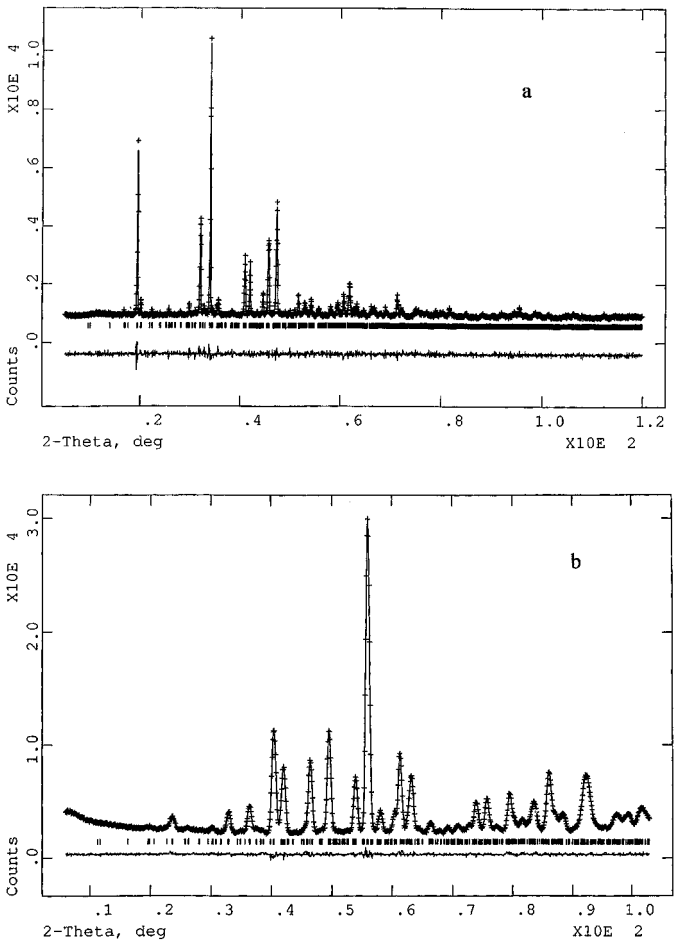

FIG. 7. Observed, calculated, and difference (a) X-ray and (b) neutron diffraction patterns for Ca_3CuMnO_6 at room temperature.

Their positions turned out to be compatible with the space group $P-1$ ($z=4$) which is a subgroup of the $C2/c$ space group and with triclinic unit cell parameters:

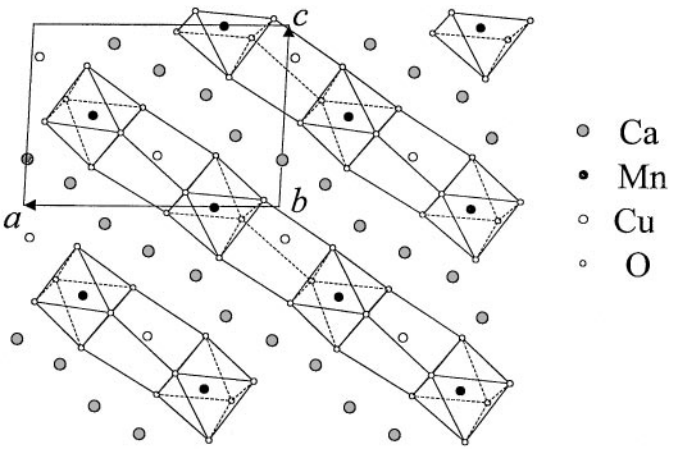

FIG. 8. Crystal structure projection of Ca_3CuMnO_6 on the (010) plane showing the unit cell of the compound and isolated chains of MnO_6 octahedra of two types and CuO_6 trigonal prisms of two types.

$a = 8.8243(4)$ Å, $b = 9.1565(4)$ Å, $c = 6.3635(3)$ Å, $\alpha = 90.203(3)^\circ$, $\beta = 92.899(3)^\circ$, $\gamma = 90.156(3)^\circ$. All atoms in this triclinic cell, which is a derivative of the monoclinic cell of Sr_3CuPtO_6, are localized in common $2i$ sites. A sharp global minimum in isotropic approximation of thermal parameters for similar species atoms was obtained using the following relationships of reliability factors of X-ray and neutron diffraction profiles: $w_{R_p} = 3.47/2.28$, $R_p = 2.53/1.77$, $DWd = 0.846/1.243$, $R(F^2) = 8.56/1.58$, $\chi^2 = 1.355$. A total of 154 various parameters including profile ones were employed in the calculation. The values of individuals thermal parameters were not determined in view of the large number of parameters. Figures 7a and 7b present experimental (crosses), theoretical (solid line), and difference diffraction patterns obtained on the basis of X-ray and neutron diffraction measurements, respectively. A projection of the crystal structure on the (010) plane in given in Fig. 8. The results of

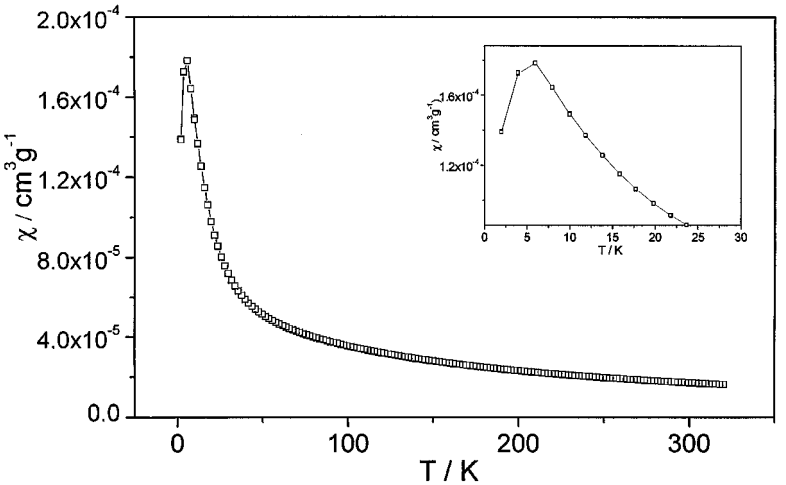

FIG. 9. Magnetic susceptibility χ as a function of temperature for Ca_3CuMnO_6.

TABLE 5
Bond distances in Ca_3CuMnO_6
(Standard Deviation in Parenthesis)

Atom	Distances, Å	Atoms	Distances, Å
Ca1–O1	2.567(26)	Ca6–O1	2.475(23)
Ca1–O3	2.440(23)	Ca6–O2	2.574(26)
Ca1–O4	2.775(26)	Ca6–O5	2.314(26)
Ca1–O7	2.538(24)	Ca6–O5	2.463(28)
Ca1–O8	2.448(25)	Ca6–O6	2.298(29)
Ca1–O11	2.504(27)	Ca6–O6	2.560(25)
Ca1–O12	2.531(28)	Ca6–O11	2.702(23)
Ca1–O13	2.308(25)	Ca6–O12	2.679(26)
Ca2–O2	2.637(23)	Mn1–O1	1.954(24)
Ca2–O2	2.778(25)	Mn1–O3	1.883(20)
Ca2–O2	2.370(27)	Mn1–O5	1.984(26)
Ca2–O2	2.310(29)	Mn1–O7	1.869(25)
Ca2–O2	2.584(26)	Mn1–O9	1.975(23)
Ca2–O2	2.427(24)	Mn1–O11	1.911(24)
Ca2–O2	2.294(25)		
Ca2–O2	2.518(29)	Mn2–O2	1.909(25)
		Mn2–O4	1.863(23)
Ca3–O1	2.247(26)	Mn2–O6	1.982(26)
Ca3–O2	2.483(20)	Mn2–O8	1.748(21)
Ca3–O3	2.333(24)	Mn2–O10	1.937(22)
Ca3–O5	2.645(27)	Mn2–O12	1.984(22)
Ca3–O6	2.407(26)		
Ca3–O9	2.559(28)	Cu1–O3	2.101(22)
Ca3–O10	2.502(26)	Cu1–O4	2.399(23)
Ca3–O10	2.385(25)	Cu1–O5	2.206(24)
		Cu1–O6	2.080(20)
Ca4–O1	2.383(27)	Cu1–O11	2.319(22)
Ca4–O2	2.459(26)	Cu1–O12	2.101(22)
Ca4–O4	2.401(25)		
Ca4–O5	2.405(29)	Cu2–O1	2.569(19)
Ca4–O6	2.502(23)	Cu2–O2	1.914(23)
Ca4–O9	2.414(24)	Cu2–O7	2.1543(25)
Ca4–O9	2.346(22)	Cu2–O8	2.101(23)
Ca4–O10	2.490(25)	Cu2–O9	1.946(26)
		Cu2–O10	2.540(19)
Ca5–O3	2.449(26)		
Ca5–O4	2.362(25)	Mn1–Cu1	2.689(17)
Ca5–O7	2.393(26)	Mn1–Cu2	2.688(14)
Ca5–O7	2.530(27)	Mn2–Cu1	2.639(15)
Ca5–O8	2.478(23)	Mn2–Cu2	2.759(17)
Ca5–O8	2.492(24)		
Ca5–O9	2.683(25)		
Ca5–O10	2.588(26)		

combined refinement of the crystal structure of Ca_3CuMnO_6 are listed in Table 4. In contrast to Sr_3CuPtO_6, Ca_3CuMnO_6 is characterized by the presence of two types of sites both for Cu and Mn atoms. From the computation of atomic sites' occupation (Table 4) it follows that Cu1 sites are 90% occupied by copper and 10% by manganese, whereas Cu2 sites are 100% occupied by copper. Table 5 presents the main cation–anion interatomic distances for Ca_3CuMnO_6. Copper atoms of two species (Cu1 = 0.9Cu + 0.1Mn, Cu2 = Cu) are inside the trigonal prisms. However, analysis of copper–oxygen interatomic distances shows that the coordination number (4 + 2) is characteristic virtually of both species of copper atoms. If we assume a square-planar surrounding (coordination number 4), the mean copper–oxygen distances in Cu1 and Cu2 sites are 2.122 and 2.026 Å, respectively. Such a surrounding is a manifestation of the Jahn–Teller effect exhibited by bivalent copper cations. Since Cu1 sites are 10% occupied by manganese, the Jahn–Teller effect is partially suppressed. This is accompanied by an increase in the mean cation–anion distance (2.122 Å) for coordination number 4 and by a displacement of these atoms to the center of the trigonal prism. For this case (coordination number 4 + 2) the mean Cu1–O distance is 2.201 Å. At the same time Cu2 atoms are practically in the center of the side face of the trigonal prism. The mean Cu2–O distance for coordination number 4 (2.026 Å) is similar to those found for Sr_3CuPtO_6 (2.007 and 2.017 Å) (18). Two types of manganese atoms (Mn1 and Mn2) are inside octahedral with mean manganese–oxygen distances of 1.929 and 1.904 Å, respectively. These values are in good agreement with those observed in Ca_3NiMnO_6 (4) and Ca_3CoMnO_6 (1.905 Å).

The crystal lattice of this compound contains six species of calcium atoms localized inside distorted square antiprisms (coordination number 8). The mean Ca–O distances change from 2.425 to 2.513 Å. As follows from Fig. 8, the combination of edge-shared octahedra and trigonal prisms gives rise to isolated zigzag chains of alternating copper and manganese atoms ...Mn1Cu1Mn2Cu2Mn1... etc. These chains are separated from each other by columns of distorted square oxygen antiprisms with Ca atoms inside them.

It is interesting to compare the structure of Ca_3CuMnO_6 with the structures of other low-dimensional Cu-containing oxides, in particular Sr_3CuIrO_6 (5) and $Ba_6CuMn_4O_{15}$ (20). As indicated above, the symmetry of the former compound decreased to monoclinic ($C2/c$). This is due to the fact that Cu cations are displaced from the center of trigonal-prismatic positions into one of the rectangular faces of the polyhedron. In this oxide Cu is completely ordered in the square-planar faces. However, the symmetry of the latter compounds is not lowered. The reason for this, in the opinion of the authors (20), is that the cation disorder quenches the cooperative Jahn–Teller distortion. In this compound the trigonal-prismatic sites are 67% occupied by Cu and 33% by Mn. We have found that Ca_3CuMnO_6 has a more ordered distribution of Mn and Cu cations in octahedral and prismatic sites. As a consequence, the crystal symmetry of this oxide is lowered, too ($P-1$).

The low-temperature magnetic measurements performed showed that the temperature versus magnetic susceptibility dependence of Ca_3CuMnO_6 exhibits a clear-cut maximum at 6 K (Fig. 9) which may be indicative of a transition of the oxide to a magnetically ordered (most probably,

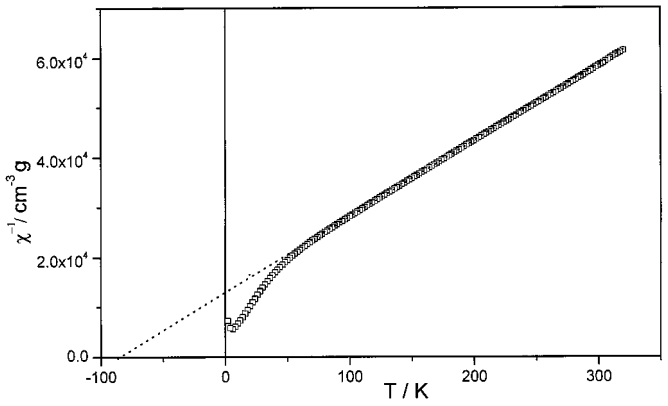

FIG. 10. Inverse magnetic susceptibility χ^{-1} as a function of temperature for Ca_3CuMnO_6.

antiferromagnetic) state. The magnetic susceptibility χ of Ca_3CuMnO_6 obeys the Curie–Weiss law $\chi = C/(T - \theta)$ above 50 K (Fig. 10). Constants C and θ from the Curie–Weiss equation equal 2.28 and -85 K, respectively. The effective magnetic moment (4.27 μ_B) is close to the theoretical one for the cation combination Cu^{2+}–Mn^{4+} (4.24 μ_B). The dependence between magnetization and magnetic field is of a linear character both below and above 6 K, which is indicative of the absence of a spontaneous magnetic moment in Ca_3CuMnO_6.

Thus, the aforesaid shows that Ca_3CuMnO_6 is the first representative of compounds from the $A_{3n+3}A'_nB_{3+n}O_{9+6n}$ family (19) ($n = \inf$, structural type Sr_4PtO_6) with a triclinic crystal lattice (space group $P-1$, $z = 4$). Magnetic susceptibility studies performed give us grounds to assume that the long-range magnetic order (apparently antiferromagnetic) is possible in this compound below 6 K.

ACKNOWLEDGMENTS

This work was supported by the Russian Foundation for Basic Research (grants no. 00-15-97418 and 98-03-32697a).

REFERENCES

1. G. V. Bazuev, V. G. Zubkov, V. N. Krasilnikov, K. N. Mikhalev, and T. I. Arbuzova, *Dokl. Akad. Nauk* (*Russia*) **363**(5), 634 (1998).
2. G. V. Bazuev, V. N. Krasilnikov, V. G. Zubkov, I. F. Berger, and T. I. Arbuzova, "Book of Abstracts of 5th International Workshop on High-Temperature Superconductors and Novel Inorganic Materials Engineering (MSU HTSC-V)," Moscow State University, Moscow, W-39, 1998.
3. G. V. Bazuev, V. G. Zubkov, I. F. Berger, and T. I. Arbuzova, *Z. Neorg. Khim.* **45**(7), 1204 (2000).
4. G. V. Bazuev, V. G. Zubkov, I. F. Berger, and T. I. Arbuzova, *Solid State Sci.* **1,** 365 (1999).
5. T. N. Nguyen, P. A. Lee, and H.-C. zur Loye, *Science* **271**(5248), 489 (1996).
6. T. N. Nguyen and H.-C. zur Loye, *J. Solid State Chem.* **117**(1), 300 (1995).
7. H. Fjellvag, E. Gulbransen, S. Aasland, A. Olsen, and B. C. Hauback, *J. Solid State Chem.* **124**(1), 190 (1996).
8. H. Kageyama, K. Yoshimura, K. Kosuge, M. Azuma, M. Takano, H. Mitamura, and T. Goto, *J. Phys. Soc. Jpn.* **66**(12), 3996 (1997).
9. A. C. Larson and R. B. Von Dreele, "GSAS Lansce, MS-H805," Los Alamos Natl. Lab., Los Alamos, NM 87545 (April 21, 1995).
10. R. D. Shannon, *Acta Crystallogr., Sect. A.* **32**(5), 751 (1976).
11. N. Mizutani, A. Kitazawa, N. Onkuma, and M. Kato, *Kogyo Kogaku Zasshi* **43**(6), 1097 (1970).
12. J.-C. Bouloux, J.-L. Soubeyroux, G. Le Flem, and P. Hagenmuller, *J Solid State Chem.* **38**(1), 34 (1981).
13. I. D. Brown and D. Altermatt, *Acta Crystallogr., Sect. B* **41,** 244 (1985).
14. B. N. Figgis, *Nature* **182,** 1568 (1958).
15. G. Blasse, *J. Phys. Chem. Solids* **26**(12), 1969 (1965).
16. K. Asai, K. Fujiyoshi, N. Nishimori, Y. Satoh, Y. Kobayashi, and M. Mizoguchi, *J. Phys. Soc. Jpn.* **67**(12), 4218 (1988).
17. A. P. Wilkinson, A. K. Cheetam, W. Kunnman, and A. Kvick, *Eur. J. Solid State Inorg. Chem.* **28,** 453 (1991).
18. J. L. Hodeau, H. Y. Tu, P. Bordet, T. Fournier, P. Strobel, M. Marezio, and G. V. Chandrashekhar, *Acta Crystallogr., Sect. B* **48,** 1 (1992).
19. J. Darriet and M. A. Subramanian, *J. Mater. Chem.* **5**(4), 543 (1995).
20. E. J. Cussen, J. F. Vente, and P. D. Battle, *J. Am. Chem. Soc.* **121**, 3958 (1999).